

Parton densities and structure functions at next-to-next-to-leading order and beyond

W.L. van Neerven and A. Vogt

Instituut-Lorentz, University of Leiden,
P.O. Box 9506, 2300 RA Leiden, The Netherlands

Abstract. We summarize recent results on the evolution of unpolarized parton densities and deep-inelastic structure functions in massless perturbative QCD. Due to last year's extension of the integer-moment calculations of the three-loop splitting functions, the NNLO evolution of the parton distributions can now be performed reliably at momentum fractions $x \gtrsim 10^{-4}$, facilitating a considerably improved theoretical accuracy of their extraction from data on deep-inelastic scattering. The NNLO corrections are not dominated, at relevant values of x , by their leading small- x terms. At large x the splitting-function series converges very rapidly, hence, employing results on the three-loop coefficient functions, the structure functions can be analysed at N³LO for $x > 10^{-2}$. The resulting values for α_s do not significantly change beyond NNLO, their renormalization scale dependence reaches about $\pm 1\%$ at N³LO.

1. Introduction

Precise predictions for hard strong-interaction processes require transcending the standard next-to-leading order (NLO) approximation of perturbative QCD. Resummations of large logarithms may be sufficient for specific processes, but generally full next-to-next-to-leading order (NNLO) calculations are called for. For electron–proton scattering and proton–(anti-)proton colliders this demands both partonic cross sections and parton distribution of NNLO accuracy.

The former quantities are presently available only for the structure functions in deep-inelastic scattering (DIS) [1] – which provide the backbone of our knowledge of the proton’s parton densities and are among the quantities best suited for measuring α_s – and the total cross section for the Drell-Yan process [2] – which in the form of W and Z production is an excellent candidate for an accurate luminosity monitor at TEVATRON and the LHC [3]. The calculation of other processes like jet production at NNLO is under way, e.g., the required two-loop two-to-two matrix elements have been computed [4] using the pioneering results [5] for the scalar double-box diagrams. See refs. [6] for recent brief overviews. Partial NNLO results (the soft- and virtual-gluon contributions) have also been obtained for Higgs production via gluon-gluon fusion in the heavy top-quark limit [7], see also ref. [8].

The three-loop splitting functions entering the NNLO evolution of the parton distributions have not been completed so far either [9]. However, previous partial results [10, 11] have been substantially extended by the calculation of two more Mellin moments [12]. In Section 2 we discuss the resulting improvement [13] of our approximations of the splitting functions in x -space [14], and compare, in the extended range $x \gtrsim 10^{-4}$ of safe applicability, the resulting approximate NNLO flavour-singlet evolution and its scale stability to the NLO results. We also briefly re-address [15, 16] the question to what extent the leading small- x contributions to the splitting functions and coefficient functions dominate the small- x evolution.

Taking into account the fast convergence of the splitting-function series shown in Section 2, the next-to-next-to-next-to-leading order (N³LO) corrections for the DIS structure functions can be effectively derived at $x > 10^{-2}$ using available partial results [10, 12, 18] for the three-loop coefficient functions. The effect of the NNLO and N³LO terms is discussed in Section 3 for the scaling violations of the non-singlet structure function F_2 and the resulting determination of α_s [19]. Here we also illustrate the predictions of the principle of minimal sensitivity [20], the effective charge method [21] and the Padé summation [22] which in this case, unlike the soft-gluon resummation, seem to facilitate a reliable estimate of the corrections even beyond N³LO.

A first study has been performed [23] of the effects of the NNLO corrections (using our original approximations [14] for the three-loop splitting functions) in a global parton analysis. See refs. [24, 25] for beyond-NLO α_s analyses of DIS data using methods more directly based on the integer-moment results [10, 12].

2. Singlet parton densities and structure functions at NNLO

We first illustrate our approximation procedure for the three-loop splitting functions $P^{(2)}$. As an example we discuss the N_f^1 term $P_{qg,1}^{(2)}$ of the gluon-quark splitting function P_{qg} dominating the small- x evolution of the quark densities. In the $\overline{\text{MS}}$ scheme employed in our studies, this function can be written as

$$P_{qg,1}^{(2)}(x) = \sum_{m=1}^4 A_m \ln^m(1-x) + f_{\text{smooth}}(x) + \sum_{n=1}^4 B_n \ln^n x + \sum_{p=0}^1 C_p \frac{\ln^p x}{x}. \quad (1)$$

The leading small- x coefficient C_1 has been derived by Catani and Hautman [11]. The function f_{smooth} collects all contributions which are finite for $0 \leq x \leq 1$. This regular term constitutes the mathematically complicated part of Eq. (1), involving higher transcendental functions like the harmonic polylogarithms [26].

For our improved approximations [13] we choose three or two of the large- x logarithms in Eq. (1), a one- or two-parameter smooth function (low powers or simple polynomials of x) and two of the small- x terms (x^{-1} together with $\ln x$ or $\ln^2 x$). Their coefficients are then determined from the six even-integer Mellin moments

$$P_{qg,1}^{(2)}(N) = \int_0^1 dx x^{N-1} P_{qg,1}^{(2)}(x) \quad (2)$$

computed by Larin et al. [10] and Retey and Vermaseren [12]. By varying these choices we arrive at about 50 approximations (see Fig. 1 of ref. [13]). The two functions spanning the resulting error band for most of the x -range are finally selected as our best estimates for $P_{qg,1}^{(2)}(x)$ and its residual uncertainty.

These two functions, denoted by ‘A’ and ‘B’, are shown in Fig. 1 together with their (practically indistinguishable) real moments (2) for $2 \lesssim N \leq 30$ and their convolutions

$$[P_{qg}^{(2)} \otimes g](x) = \int_x^1 \frac{dy}{y} P_{qg}^{(2)}(y) g\left(\frac{x}{y}\right) \quad (3)$$

with a typical gluon distribution g . In Figs. 1(b) and 1(c) the corresponding results for the N_f^2 term have been supplemented for $N_f = 4$. Note that, like refs. [10, 12], we use the small expansion parameter $a_s = \alpha_s/(4\pi)$; scaling down the ordinates by a factor 2000 yields the results for an expansion in α_s . The large impact of the $N = 10$ and 12 moments [12] is illustrated by also showing our less accurate, but compatible original approximations [14] based on the four lowest even-integer moments [10].

Knowing the leading $x^{-1} \ln x$ term [11] is clearly instrumental in constraining the small- x behaviour of $P_{qg,1}^{(2)}$ – something not efficiently done by a small number of $N \geq 2$ integer moments (2). However, even at $x \leq 10^{-3}$ where the non- x^{-1} parts contribute less than 10% to both approximations ‘A’ and ‘B’, this term does not sufficiently dominate over the (so far uncalculated) subleading $C_0 x^{-1}$ contribution in Eq. (1), leaving us with a sizeable uncertainty of $P_{qg,1}^{(2)}$ for $x \lesssim 10^{-2}$. We will examine the dominance of the $x^{-1} \ln x$ and x^{-1} terms for the convolution (3), which in any case considerably smoothes out the oscillating differences of the approximations, at the end of this section.

After applying analogous procedures to the other three-loop splitting functions (see Figs. 2 and 3 of ref. [13]) we are ready to exemplify the effect of the NNLO contributions

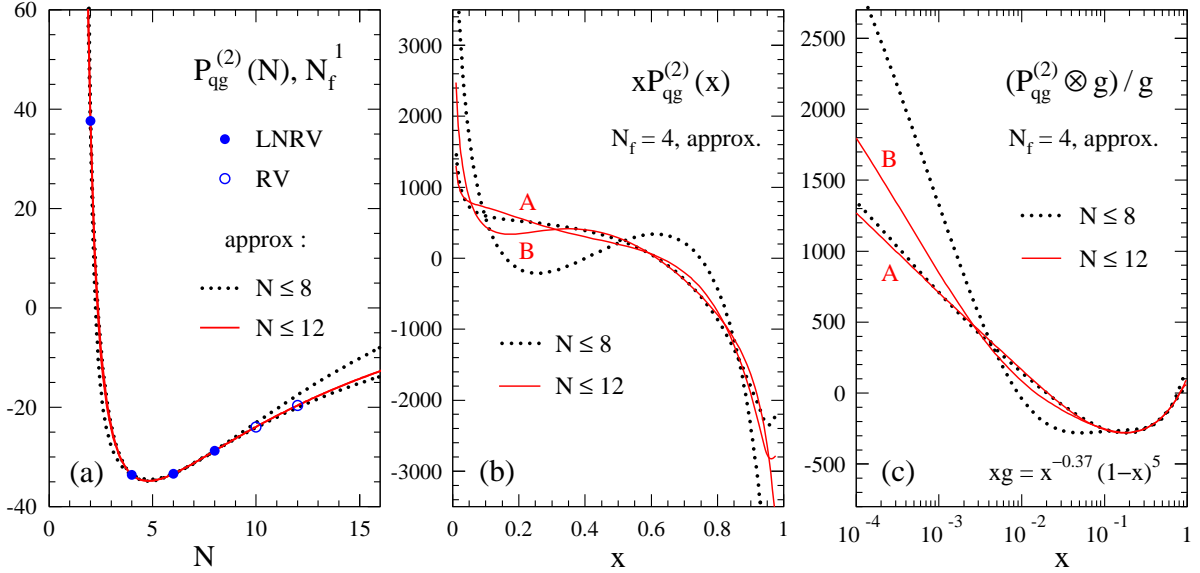


Figure 1. (a) Exact results [10, 12] (points) and approximations [14, 13] (curves) for the moments of the N_f^1 term of the three-loop gluon-quark splitting function in the $\overline{\text{MS}}$ scheme. (b) The approximations in x -space for $N_f = 4$, and (c) their normalized convolutions with a typical gluon distribution.

on the evolution of the parton densities. This is done in Fig. 2 via the logarithmic factorization-scale derivatives $\dot{f} = d \ln f / d \ln \mu_f^2$ of the typical singlet quark (Σ) and gluon (g) distributions

$$\begin{aligned} x\Sigma(x, \mu_{f,0}^2) &= 0.6 x^{-0.3} (1-x)^{3.5} (1+5x^{0.8}) \\ xg(x, \mu_{f,0}^2) &= 1.0 x^{-0.37} (1-x)^5 \end{aligned} \quad (4)$$

at the reference scale

$$\mu_f^2 = \mu_{f,0}^2 \approx 30 \text{ GeV}^2 \quad \longleftrightarrow \quad \alpha_s(\mu_{f,0}^2) = 0.2 . \quad (5)$$

In Fig. 2(a) the resulting relative NNLO effects are shown for the standard choice $\mu_r = \mu_f$ of the renormalization scale. Note that the spikes close to $x = 0.1$ do not represent large NNLO corrections, instead they derive from zeros of the denominators. In fact, the NNLO corrections are very small (except for the quark evolution at small x), much smaller than their NLO counterparts not shown in the figure (except for the gluon evolution at small x , where already the NLO corrections are rather small). Consequently, as illustrated in Figs. 2(b) and 2(c), the renormalization-scale stability of the prediction is considerably improved over the full x -range. If measured over the conventional range $1/2 \mu_f \leq \mu_r \leq 2 \mu_f$, the μ_r dependence of $\dot{\Sigma}$ amounts to less than $\pm 2\%$ at large x and $\pm 5\%$ small x , that of \dot{g} to less than $\pm 1\%$ and $\pm 2\%$, respectively.

Also displayed in Fig. 2 are the present inaccuracies (‘A’ vs. ‘B’) of the NNLO results caused by the remaining uncertainties [13] of the three-loop splitting functions. These inaccuracies are entirely negligible at large x . Down to $x \simeq 10^{-4}$ they amount to about $\pm 2\%$ or less with respect to the central results not shown in the figure, even

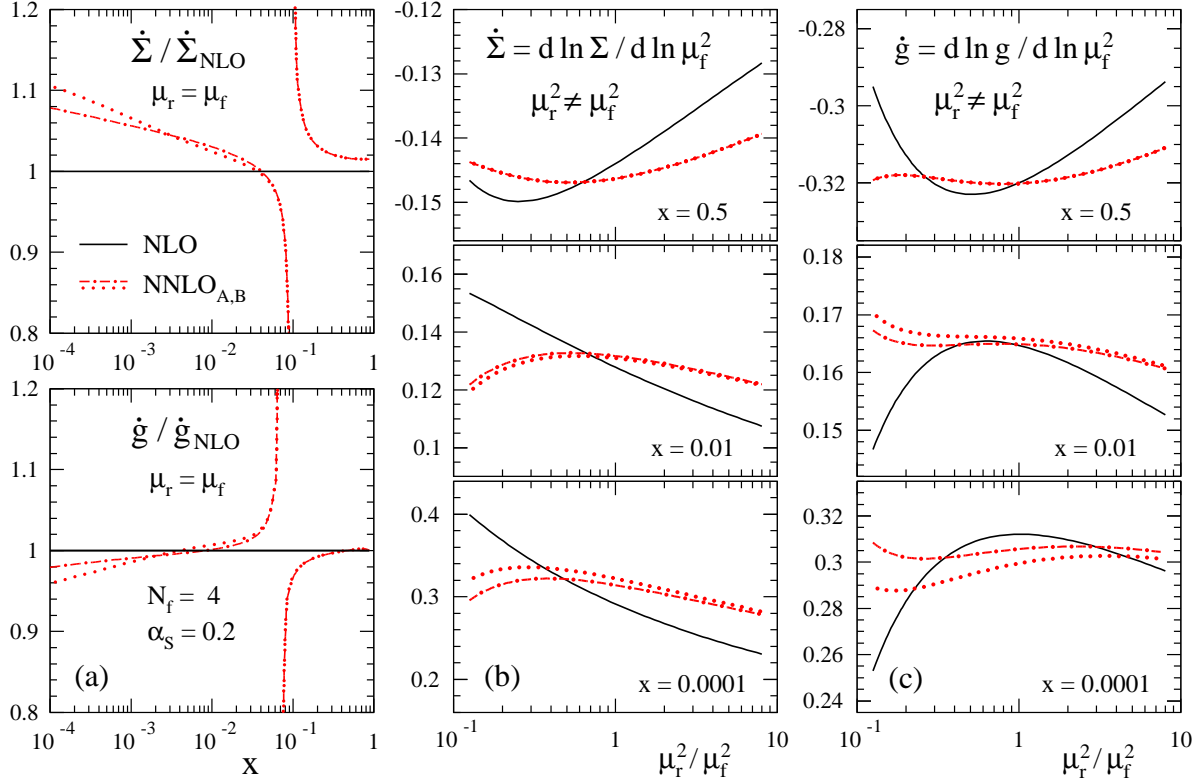


Figure 2. (a) Size and present approximation uncertainties of the NNLO corrections to the scale derivatives of the singlet quark and gluon densities for the input (4) and (5) at $\mu_r = \mu_f$. (b,c) The renormalization scale dependence at NLO and NNLO for three typical values of x .

if the bands in Fig. 2(a) are increased by 50% in order to account for any possible underestimate of the uncertainties.

At lower scales the splitting-function uncertainties have a larger impact, mainly due to the larger value of α_s . For example, the spread corresponding to Fig. 2(a) reaches about $\pm 4\%$ for $\dot{\Sigma}$ and $\pm 3\%$ for \dot{g} at $x = 10^{-4}$ and $\mu_f^2 \approx 3 \text{ GeV}^2$ corresponding to $\alpha_s = 0.3$. In view of the also enhanced NLO scale dependence, the approximate NNLO evolution represents an improvement over the NLO treatment even with inaccuracies of this size.

The electromagnetic singlet structure function F_2 and its Q^2 derivatives are presented in Fig. 3 for the parton densities (4) at $Q^2 = \mu_{f,0}^2 \approx 30 \text{ GeV}^2$. The large NNLO corrections at very large x originate in the non-singlet part of the two-loop quark coefficient function. Note, however, that the (positive) gluon contribution to $dF_{2,S}/d \ln Q^2$ at NNLO still amounts to 5% at $x = 0.5$ (40% more than at NLO), and falls below 1% only above $x = 0.7$ [14]. This effect is large enough to jeopardize analyses applying a non-singlet formalism to the proton's F_2 in the region $x > 0.3$.

The negative NNLO corrections to F_2 at small x arise from the two-loop gluon coefficient function $c_{2,g}^{(2)}$. The Q^2 derivative, on the other hand, receives a +10% NNLO correction for $10^{-4} \lesssim x \lesssim 10^{-2}$; its break-up is illustrated in Fig. 3(a) by the results for $P^{(2)} = 0$. Also for F_2 and its scaling violations the inclusion of the NNLO terms leads to

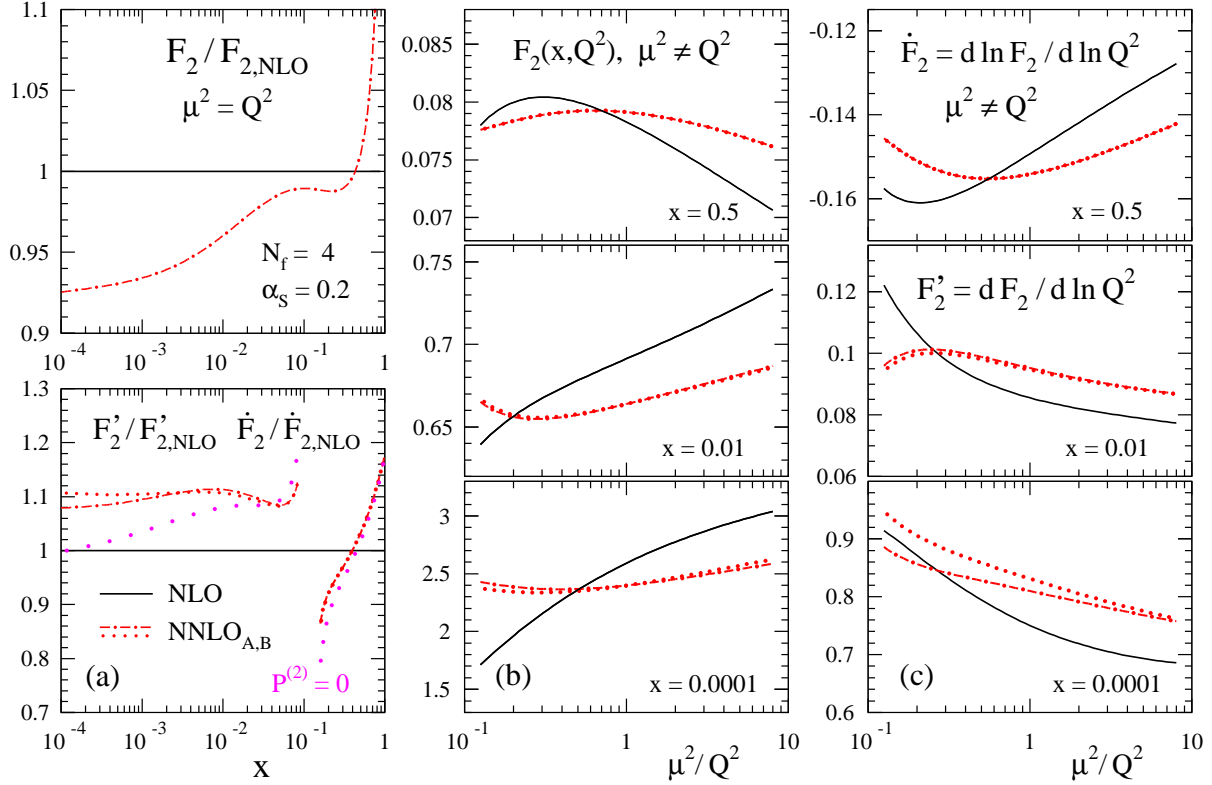


Figure 3. (a) The NNLO corrections for the singlet F_2 and its Q^2 derivatives (linear at small x , logarithmic at large x) for the input (4) at $\mu_r^2 = \mu_f^2 \equiv \mu^2 = \mu_{f,0}^2 = Q^2 \approx 30 \text{ GeV}^2$. (b,c) The scale dependence at NLO and NNLO for three typical values of x .

a substantial decrease of the scale uncertainties as shown in Figs. 3(b,c), which facilitates more precise extractions of the parton distributions from data on these quantities.

We conclude this section by examining the dominance of the small- x terms of the NNLO splitting functions and coefficient functions for the small- x convolutions. In Fig. 4 the results for $f \otimes g$, $f = P_{gg}^{(2)}$, $P_{qg}^{(2)}$ and $c_{2,g}^{(2)}$ obtained by keeping only the $x^{-1} \ln^k x$ terms of f are compared, down to $x = 10^{-6}$, with the (for $P^{(2)}$ approximate) full results. The dependence on the gluon distribution g is illustrated by employing, besides our ‘steep’ standard input (4), also a low-scale ‘flat’ shape, $xg \sim x^0$ for $x \rightarrow 0$.

Keeping only the leading $x^{-1} \ln x$ terms [11] of $P_{gg}^{(2)}$ and $P_{qg}^{(2)}$ does not lead to reasonable approximations as shown in Figs. 4(a,b), regardless of the gluon distribution. Even for the more favourable flat shape the offsets amount to about a factor of two even at $x = 10^{-6}$. Besides the x^{-1} contributions, the non- x^{-1} terms do not seem to be sufficiently suppressed either, at least for a steep gluon distribution. Due to the present large uncertainties [13] on the x^{-1} terms, however, definite conclusions especially for a flat gluon distribution require the computation [9] of the exact x -dependence of $P_{ij}^{(2)}$. On the other hand, such conclusions can be drawn already [15] for the convolutions of the two-loop coefficient function $c_{2,g}^{(2)}$ [1] shown in Fig. 4(c). The leading x^{-1} term [11] does not dominate over the non- x^{-1} contributions at any x -values of practical interest.

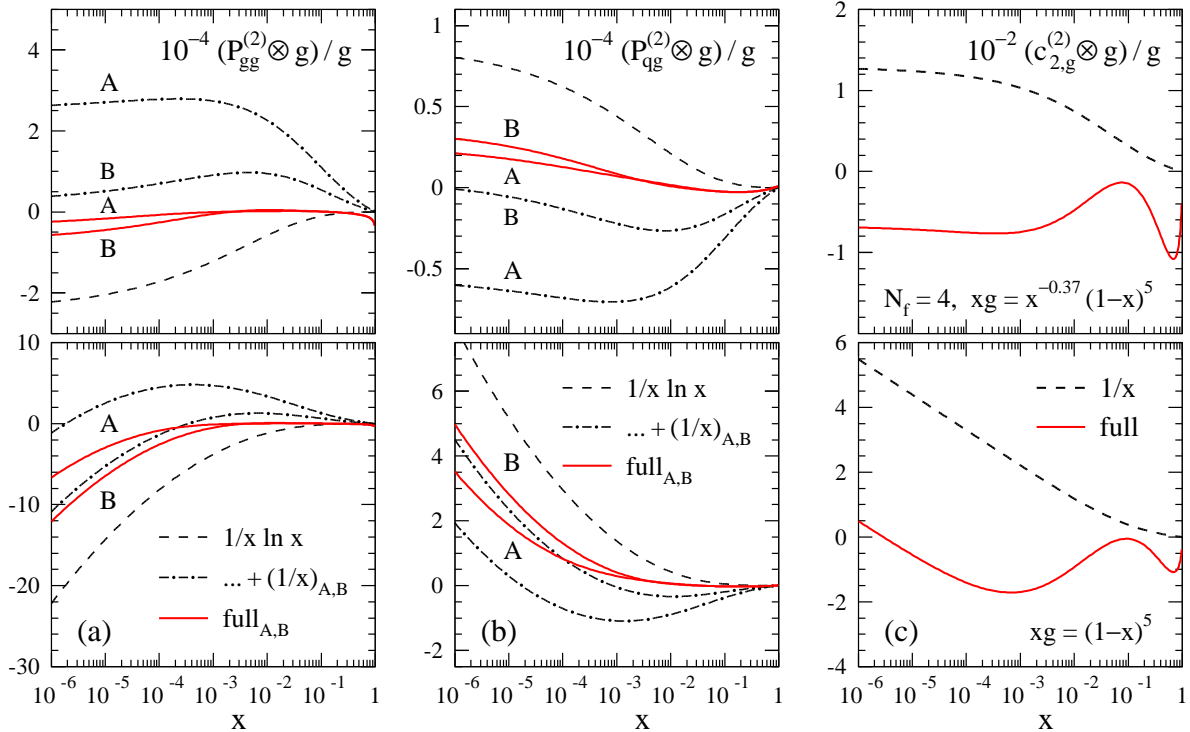


Figure 4. The convolutions of the leading (and, for $P^{(2)}$, subleading) small- x terms of (a,b) the NNLO splitting functions $P_{gg}^{(2)}$ and $P_{qg}^{(2)}$ and (c) the NNLO coefficient function $c_{2,g}^{(2)}$ with two typical ‘steep’ (upper row) and ‘flat’ (lower row) gluon distributions, compared to the respective (for $P^{(2)}$) approximate) full results.

3. Non-singlet structure functions at NNLO and beyond

The scaling violations of the non-singlet structure functions $F_{a,\text{NS}}$, $a = 1, 2, 3$, can be conveniently discussed in terms of the physical evolution kernels $K_{a,\text{NS}}$,

$$\frac{d}{d \ln Q^2} F_{a,\text{NS}} = K_{a,\text{NS}} \otimes F_{a,\text{NS}} = \sum_{l=0} a_s^{l+1} K_{a,l} \otimes F_{a,\text{NS}}. \quad (6)$$

The $N^l\text{LO}$ expansion coefficients $K_{a,l}$ are combinations of the coefficient functions up to l loops and the splitting functions up to $l+1$ loops. See Eqs. (2.7) – (2.9) of ref. [19] for the details. The advantage of Eq. (6) is that any dependence on the factorization scheme and the scale μ_f has been eliminated explicitly. Note, however, that in α_s analyses in terms of coefficient functions and parton distributions the main uncertainty arises from the dependence on the renormalization scale μ_r , not the factorization scale μ_f .

The NNLO kernels $K_{a,2}$ are fixed by the two-loop coefficient functions [1] (for which compact parametrizations are available [14]) together with our approximations [13] for three-loop splitting functions. The uncertainties of the latter are negligible in the region $x > 10^{-2}$ in which we are mainly interested for the non-singlet case.

Due to the fast large- x convergence of the splitting function series illustrated in Fig. 2, the $N^3\text{LO}$ kernels are dominated by the coefficient functions. The seven lowest even (for $F_{1,2}$) and odd (for F_3) moments at three loops have been computed by Larin

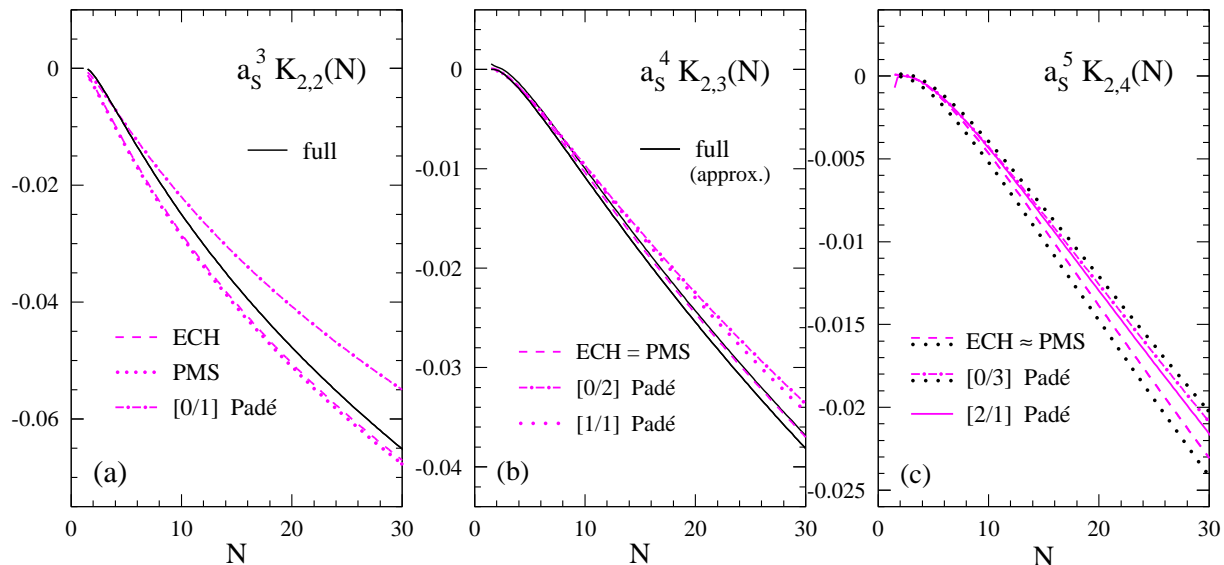


Figure 5. The PMS, ECH and Padé estimates of (a) the NNLO, (b) the N³LO, and (c) the N⁴LO contributions to the N -space evolution kernel for $\frac{1}{x}F_{2,\text{NS}}$ at $\mu_r^2 = Q^2$, $N_f = 4$ and $\alpha_s = 0.2$. Also shown are the (approximate) full NNLO and N³LO results.

et al. [10] ($N \leq 10$ for $F_{1,2}$) and Retey and Vermaseren [12]. When complemented by the four leading large- x terms $(1-x)^{-1} \ln^k(1-x)$, $k = 2, \dots, 5$ derived [18] from the soft-gluon resummation [17], this information facilitates x -space approximations (analogous to those for $P^{(2)}$ exemplified in Section 2) which are sufficiently accurate in the above-mentioned region of x , as shown in Figs. 2 and 3 of ref. [19]. The small effect of the uncalculated four-loop splitting functions $P^{(3)}$ can be estimated by assigning a 100% error to the Padé prediction $P_{\text{NS}}^{(3)}(N) \approx P_{\text{NS}}^{(3)}(N)_{[1/1] \text{ Padé}}$. Actually the small residual uncertainties of $K_{a,3}$ at $x > 10^{-2}$ are dominated by this error, not by the approximation uncertainties [19] of the three-loop coefficient functions.

Knowing the evolution kernels to such a high order also facilitates a test of the predictions for $K_{a,l}$ derived from the Padé summation [22] of the perturbation series and from renormalization-scheme optimizations like the principle of minimal sensitivity (PMS) [20] and the effective charge (ECH) method [21]. In Figs. 5(a) and 5(b) these predictions are compared to the (approximate) full kernels $K_{2,2}$ and $K_{2,3}$ for $F_{2,\text{NS}}$ in N -space. The estimates by all these methods agree rather well for the α_s^5 (N⁴LO) contribution shown in Fig. 5(c). Such an agreement is usually interpreted [22] as evidence for the approximate correctness of the predictions.

The large- N / large- x behaviour of the kernels $K_{a,\text{NS}}$ is dominated by the soft-gluon terms $a_s^{l+1} \ln^k N$, $1 \leq k \leq l+1$. The soft-gluon resummation [17] at next-to-next-to-leading logarithmic accuracy [18] fixes the coefficients of the leading three terms at all orders. However, as shown in Figs. 8 and 9 of ref. [19], these contributions do not provide quantitative predictions for $K_{a,l}$ at practically relevant values of N/x , due to the (quite generally, see ref. [27]) large coefficients of subleading logarithms at higher orders [18].

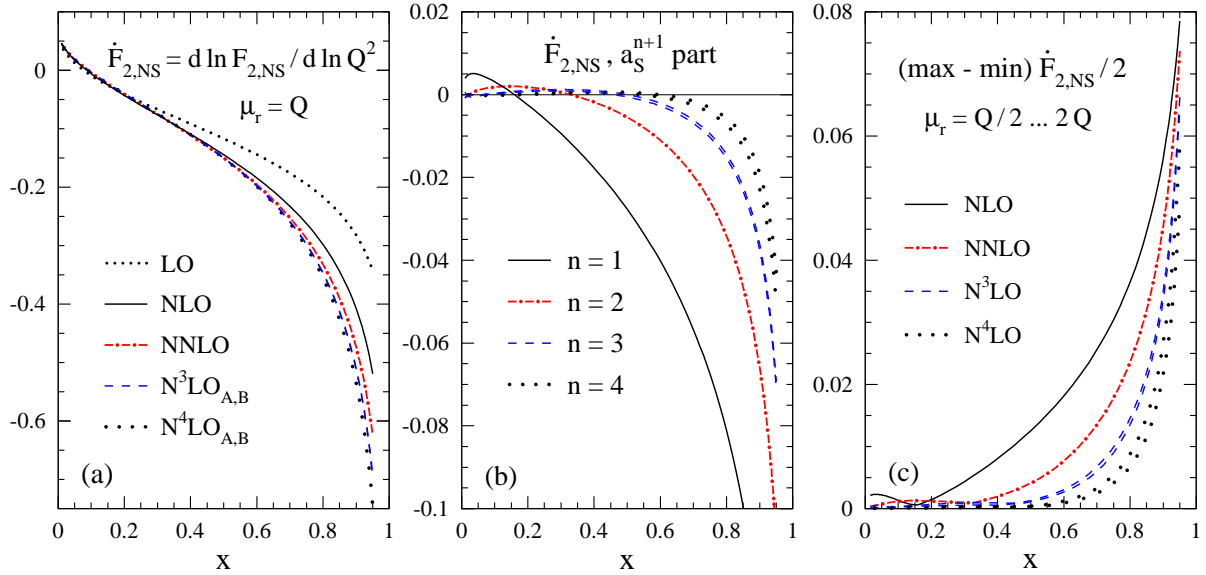


Figure 6. (a) The perturbative expansion of the logarithmic Q^2 derivative of $F_{2,NS}$ for the input (7) for $N_f = 4$ and $\mu_r^2 = Q^2$. (b) The N^nLO contributions, $n = 1 \dots 4$, to the results shown in (a), and (c) their renormalization scale uncertainties.

The effect of the higher-order terms (using the Mellin inverse of Fig. 5(c) at N^4LO , see Fig. 12 of ref. [19] for the Padé estimates of the corrections beyond N^4LO) is exemplified in Fig. 6 for the logarithmic Q^2 derivative of

$$F_{2,NS}(x, Q_0^2 \approx 30 \text{ GeV}^2) = x^{0.5}(1-x)^3, \quad \alpha_s(Q_0^2) = 0.2. \quad (7)$$

Also shown are the renormalization-scale uncertainties estimated using the conventional interval $\frac{1}{4}Q^2 \leq \mu_r^2 \leq 4Q^2$. The α_s^4 (N^3LO) corrections and the N^3LO scale dependence are very small at $x < 0.6$; they both reach about 2% and 5% of the total results only at $x = 0.65$ and 0.85 , respectively. The corresponding numbers at N^4LO read 1% and 3%.

Sample fits of α_s to the Q^2 derivatives at $0.05 \leq x \leq 0.75$ for $Q^2 = Q_0^2$ (using the N^3LO predictions of Eq. (7) as model data) yield [19]

$$\begin{aligned} \alpha_s(Q_0^2)_{NLO} &= 0.2080 \begin{matrix} + 0.021 \\ - 0.013 \end{matrix}, & \alpha_s(Q_0^2)_{NNLO} &= 0.2010 \begin{matrix} + 0.008 \\ - 0.0025 \end{matrix}, \\ \alpha_s(Q_0^2)_{N^3LO} &= 0.2000 \begin{matrix} + 0.003 \\ - 0.001 \end{matrix}, & \alpha_s(Q_0^2)_{N^4LO} &= 0.2000 \begin{matrix} + 0.0015 \\ - 0.0005 \end{matrix}, \end{aligned} \quad (8)$$

where the errors include the above μ_r variation and, at N^3LO and N^4LO , the small approximation uncertainties. Corresponding results for F_3 can be found in ref. [19]. In both cases the N^3LO and N^4LO corrections, unlike the NNLO terms, do not cause significant shifts of the central values, but just lead to a reduction of the μ_r uncertainties which reach about $\pm 1\%$ at N^3LO .

FORTTRAN subroutines of our approximations of splitting functions [13] and non-singlet coefficient functions [19] at three loops, and of the parametrizations [14] of the two-loop coefficient functions [1] and the convolutions entering the physical evolution kernels [19] can be found at <http://www.lorentz.leidenuniv.nl/~avogt>.

Acknowledgment

This work has been supported by the European Community TMR research network ‘QCD and particle structure’ under contract No. FMRX-CT98-0194.

References

- [1] E.B. Zijlstra and W.L. van Neerven, Phys. Lett. **B272** (1991) 127; *ibid.* **B273** (1991) 476; *ibid.* **B297** (1992) 377; Nucl. Phys. **B383** (1992) 525
- [2] R. Hamberg, W.L. van Neerven and T. Matsuura, Nucl. Phys. **B359** (1991) 343; E.B. Zijlstra and W.L. van Neerven, Nucl. Phys. **B382** (1992) 11
- [3] M. Dittmar, F. Pauss and D. Zurcher, Phys. Rev. **D56** (1997) 7284; V.A. Khoze, A.D. Martin, R. Orava and M.G. Ryskin, Eur. Phys. J. **C19** (2001) 313; W.T. Giele and S.A. Keller, [hep-ph/0104053](#)
- [4] C. Anastasiou, E.W.N. Glover, C. Oleari and M.E. Tejeda-Yeomans, Nucl. Phys. **B601** (2001) 318; *ibid.* **B601** (2001) 341; [hep-ph/0101304](#); [hep-ph/0104178](#)
- [5] V.A. Smirnov, Phys. Lett. **B460** (1999) 397; J.B. Tausk, Phys. Lett. **B469** (1999) 225
- [6] W.L. van Neerven, Pramana **55** (2000) 101 ([hep-ph/0003043](#)); E.W.N. Glover, [hep-ph/0106069](#)
- [7] S. Catani, D. de Florian and M. Grazzini, JHEP 05 (2001) 025; R. V. Harlander and W. B. Kilgore, Phys. Rev. **D64** (2001) 013015
- [8] M. Krämer, E. Laenen and M. Spira, Nucl. Phys. **B511** (1998) 523
- [9] S. Moch and J.A.M. Vermaseren, Nucl. Phys. (Proc. Suppl.) **89** (200) 131, 137; S. Moch, J.A.M. Vermaseren and M. Zhou, work in progress
- [10] S.A. Larin, T. van Ritbergen, and J.A.M. Vermaseren, Nucl. Phys. **B427** (1994) 41; S.A. Larin, P. Nogueira, T. van Ritbergen, and J.A.M. Vermaseren, Nucl. Phys. **B492** (1997) 338
- [11] S. Catani and F. Hautmann, Nucl. Phys. **B427** (1994) 475; J. Blümlein and A. Vogt, Phys. Lett. **B370** (1996) 149; V.S. Fadin and L.N. Lipatov, Phys. Lett. **B429** (1998) 127; M. Ciafaloni and G. Camici, Phys. Lett. **B430** (1998) 349
- [12] A. Retey and J.A.M. Vermaseren, Nucl.Phys. **B604** (2001) 281
- [13] W.L. van Neerven and A. Vogt, Phys. Lett. **B490** (2000) 111
- [14] W.L. van Neerven and A. Vogt, Nucl. Phys. **B568** (2000) 263, *ibid.* **B588** (2000) 345; see also Nucl. Phys. (Proc. Suppl.) **89** (2000) 143
- [15] W.L. van Neerven, talk at the 1993 DESY Workshop (unpublished)
- [16] J. Blümlein and A. Vogt, Phys. Rev. **D57** (1998) 1; *ibid.* **D58** (1998) 014020; J. Blümlein, V. Ravindran, W.L. van Neerven and A. Vogt, Proceedings of DIS 98, Brussels, April 1998, eds. Gh. Coremans and R. Roosen (World Scientific 1998), p. 211 ([hep-ph/9806368](#))
- [17] G. Sterman, Nucl. Phys. **B281** (1987) 310; L. Magnea, Nucl. Phys. **B349** (1991) 703; S. Catani and L. Trentadue, Nucl. Phys. **B327** (1989) 323; *ibid.* **B353** (1991) 183; S. Catani, G. Marchesini and B.R. Webber, Nucl. Phys. **B349** (1991) 635
- [18] A. Vogt, Phys. Lett. **B471** (1999) 97; *ibid.* **B497** (2001) 228
- [19] W.L. van Neerven and A. Vogt, Nucl. Phys. **B603** (2001) 42
- [20] P. M. Stevenson, Phys. Rev. **D23** (1981) 2916
- [21] G. Grunberg, Phys. Rev. **D29** (1984) 2315
- [22] M.A. Samuel, J. Ellis and M. Karliner, Phys. Rev. Lett. **74** (1995) 4380; J. Ellis, E. Gardi, M. Karliner and M.A. Samuel, Phys. Lett. **B366** (1996) 268; Phys. Rev. **D54** (1996) 6986
- [23] A.D. Martin, R.G. Robert, W.J. Stirling and R. Thorne, Eur. Phys. J. **C18** (2000) 117-126
- [24] A.L. Kataev, G. Parente and A.V. Sidorov, Nucl. Phys. **B573** (2000) 405; [hep-ph/0012014](#); [hep-ph/0106221](#)
- [25] J. Santiago and F.J. Yndurain, Nucl. Phys. **B563** (1999) 45; [hep-ph/0102312](#)
- [26] E. Remiddi and J.A.M. Vermaseren, Int. J. Mod. Phys. **A15** (2000) 725
- [27] E. Gardi and J. Rathsman, [hep-ph/0103217](#)